Cell Biol Toxicol (2025) 41:51
https://doi.org/10.1007/s10565-025-10002-0

RESEARCH

MCM8 promotes NR4A1-mediated E2F1 transcription and facilitates renal cell carcinoma through enhancing aerobic glycolysis

Shaobo Zhang · Haoqi Miao · Tian Han · Xiangzhen Wu · Chao Liang · Jian Qian · Pengfei Shao

Received: 4 August 2024 / Accepted: 12 February 2025

Abstract Renal cell carcinoma (RCC) is a type of renal malignancy originated from the urinary tubular epithelial system. Despite its high incidence, the molecular mechanisms driving its pathogenesis remain poorly understood, limiting therapeutic advancements. This study explored the link between MCM8 and RCC progression. MCM8 displays significantly high expression in RCC tissues and was closely associated with RCC pathological staging. Knocking down endogenous MCM8 in RCC cells significantly suppressed malignant phenotypes, while simultaneously inducing apoptosis. Similarly, in vivo experiments confirmed these findings, showing a pronounced reduction in tumor growth upon MCM8 silencing. Mechanistic investigations revealed that MCM8 regulates E2F1 expression by interacting with the transcription factor NR4A1, thereby affecting E2F1 transcriptional activity. Additionally, MCM8 and E2F1 collaboratively influence aerobic glycolysis and the cellular behavior of RCC cells. In conclusion, this study identifies MCM8 as a tumor-promoting factor in RCC, with its oncogenic role potentially mediated by its regulation of E2F1 expression.

Keywords Renal cell carcinoma · MCM8 · E2F1 · Aerobic glycolysis

Introduction

Globally, renal cell carcinoma (RCC) ranks as the second most common urological cancer after bladder cancer, representing 3.8% of all cancer diagnoses (Miller et al. 2022; Siegel et al. 2024). According to GLOBOCAN 2020, the global incidence and mortality rates of RCC are 5.3 and 2.3 per 100,000 individuals, respectively (Sung et al. 2021). Due to its deep anatomical location and the lack of specific symptoms in the early stages, RCC is often diagnosed at an advanced stage. For localized RCC, surgery remains the standard treatment, offering effective disease control. However, despite surgical intervention, many patients eventually develop distant metastases, leading to unfavorable prognoses (Meng et al. 2023; Rizzo et al. 2023; Singh 2021). Recent advancements in genetic analysis and high-throughput sequencing have shifted the focus toward identifying novel therapeutic targets and developing molecularly targeted treatments (Golijanin et al. 2023; Wolf et al. 2020). Agents such as sorafenib and sunitinib have provided new hope.

Supplementary Information The online version contains supplementary material available at https://doi.org/10.1007/s10565-025-10002-0.

S. Zhang · T. Han · X. Wu · C. Liang · J. Qian · P. Shao (✉)
Department of Urology, The First Affiliated Hospital of Nanjing Medical University, Nanjing 210029, China
e-mail: spf8629@163.com

H. Miao
Nanjing Medical University, Nanjing 210029, China

Published online: 24 February 2025

However, the development of drug resistance continues to hinder the long-term success of these therapies (Posadas et al. 2017). These challenges underscore the critical need for further research into the mechanisms underlying RCC pathogenesis and for the discovery of new therapeutic strategies.

The MCM (minichromosome maintenance) protein family is crucial for several vital cellular processes, including DNA replication, meiosis, and the repair of homologous recombination (Deegan and Diffley 2016). These proteins are distinguished by common structural features, such as helicase domains, zinc finger motifs, and Walker A/B regions. Among the MCM proteins, MCM8 and MCM9 are the most recently identified and have garnered increasing interest in current research (Nishimura et al. 2012). MCM8 is a stable protein throughout the cell cycle, with both ATPase and helicase activities, playing a pivotal role in initiating replication and DNA damage repair. When DNA damage happens, MCM8 forms a complex with MCM9, which facilitates the recruitment of RAD51 to the damage site, aiding in DNA repair via homologous recombination using homologous chromosomes as templates for repair synthesis (Park et al. 2013). The MCM8-MCM9 complex is vital for maintaining genomic integrity, as it is involved in DNA replication and repair. Recent studies suggest that disrupting this complex can increase the sensitivity of cancer cells to DNA-damaging agents, such as cisplatin (Morii et al. 2019). However, the specific role of MCM8 in cancer initiation and progression is still not fully understood, underscoring the need for further investigation to clarify its function.

This study investigates the biological functions and regulatory mechanisms of MCM8 in the progression of renal cell carcinoma (RCC). Our results reveal that MCM8 expression is notably elevated in RCC tissues compared to normal tissues. Functional assays demonstrate that MCM8 silencing significantly inhibits the growth of renal carcinoma cells, enhances apoptosis, and reduces cell migration, highlighting its regulatory impact in RCC. From a mechanistic perspective, human gene expression profiling suggests that E2F1 is involved in the regulation of MCM8-driven aerobic glycolysis and RCC cell behaviors. This regulatory effect is likely mediated by the NR4A1-induced transcriptional activation of E2F1.

Materials and methods

Tissue microarray

A tissue microarray comprising primary human renal cancer tissues and normal tissues was obtained from Alena (Xi'an, China). Written informed consent was collected from all patients before surgical resections were performed. Histopathological evaluation classified the collected samples into stages I, II, III, and IV.

Cell culture and transfection

The 786-O renal carcinoma cell line was procured from the SIBCB, while A498 and ACHN cell lines were acquired from iCell Bioscience (Shanghai). Both 786-O and ACHN cells were cultured in RPMI-1640 medium (Gibco), maintained at 37 °C in a 5% CO2 humidified incubator. A498 cells were grown under identical conditions, but in MEM medium (Gibco). Lentiviral vectors, including LV-shCtrl, LV-shE2F1, and LV-shMCM8, were introduced into 786-O and A498 cells using Lipofectamine 3000. Transfection efficiency was confirmed by observing green fluorescence using a fluorescence microscope.

Immunohistochemistry analysis (IHC)

For immunohistochemical (IHC) analysis, a tissue microarray was employed. Initially, the tissue samples were baked and dewaxed with xylene and rehydration through a series of ethanol concentrations. After blocking endogenous peroxidase activity with 3% H_2O_2 for 5 min, the tissue samples were incubated overnight at 4 °C with primary antibodies (Table S1). Following washing, the samples were incubated with secondary antibody (Table S1) for 2 h at room temperature. The staining was performed using DAB reagent, and the tissues were counterstained with hematoxylin. The staining was evaluated using CaseViewer and ImageScope software. The results were classified as negative, positive, + + positive, or + + + positive. To assess Ki-67 expression in xenograft tissue sections, similar procedure was performed as mentioned before (Table S1).

Plasmid construction and lentivirus infection

ShRNAs targeting MCM8 (5'-AGGCAGCTGGAA TCTTTGATT-3') and E2F1 (5'-GGGCATCCA GCTCATTGCCAA-3') were synthesized by Yibeirui (Shanghai, China) and inserted into the BR-V-108 vector and introduced into competent E. coli cells (Tiangen) for plasmid generation. The plasmids were extracted using the EndoFree Maxi Plasmid Kit (Tiangen), following the manufacturer's instructions, and were then used for lentivirus production.

For lentiviral transduction, a multiplicity of infection (MOI) between 3 and 5 was set. Transfection was allowed to continue for 48 h to ensure efficient delivery of the shRNAs or constructs. After transfection, the medium was changed to remove any remaining viral particles. For overexpression experiments, full-length cDNAs of MCM8, E2F1, or NR4A1, which were amplified by PCR, were packaged into lentiviral vectors. Empty vectors were used as controls. All transfections were conducted in a 37 °C incubator with 5% CO_2 to maintain optimal conditions for cell growth. Transfection efficiency was assessed either by fluorescence microscopy for vectors with fluorescent markers or by qPCR to evaluate gene expression at different time points post-transfection.

qRT-PCR analysis

Total RNA was isolated from 786-O and A498 cells transduced with shRNA-expressing lentiviruses using TRIzol reagent (Sigma) and was assessed with a Nanodrop 2000/2000C spectrophotometer (Thermo Fisher Scientific). For quantitative reverse transcription PCR (qRT-PCR), a Biosystems 7500 Sequence Detection System was used, along with a SYBR Green Mastermix Kit (Vazyme). The $2^{-\Delta\Delta Ct}$ method was used for quantification. Each experiment was performed in triplicate, and the sequences for the forward and reverse primers are listed in Table S2.

Western blotting assay

786-O and A498 cells, infected with lentivirus, were lysed using ice-cold RIPA buffer (Millipore), and protein concentrations were determined with the BCA Protein Assay Kit (HyClone-Pierce). A total of 20 μg of protein was separated on 10% SDS-PAGE gels (Invitrogen) and transferred to PVDF membranes. To prevent non-specific binding, membranes were blocked with TBST containing 5% skim milk at room temperature for 1 h. Primary antibody incubation (overnight, 4 °C) and secondary antibody incubation (1 h, room temperature) (see Table S1 for antibody details) were then performed. Protein detection was done using enhanced chemiluminescence (ECL) from Amersham.

For co-immunoprecipitation (Co-IP), after centrifugation at 12,000 × g for 15 min at 4 °C to remove debris, the supernatant was collected. The lysates were incubated overnight at 4 °C with either IgG or anti-MCM8 antibodies. Protein A/G agarose beads (Beyotime, China) were added, and the mixture was gently rotated for 2–4 h. Immunocomplexes were washed three times with cold RIPA buffer to eliminate non-specific proteins. Finally, the complexes analyzed using similar procedure as mentioned above, with anti-MCM8 and anti-NR4A1 antibodies. Details of the antibodies used are provided in Table S1.

Flow cytometry for apoptosis

To evaluate apoptosis, 786-O and A498 cells were cultured in 6-well plates containing 2 mL of medium per well and cultured until reaching approximately 85% confluence. The cells were detached using trypsin, washed twice with ice-cold D-Hanks buffer (4 °C), and then centrifuged at 1000 × g, and resuspended in 1 × binding buffer. For staining, samples were added with Annexin V-APC and Propidium Iodide (PI) (5 μL each) and maintained in dark at room temperature. After 15 min, apoptosis was assessed using a FACSCalibur flow cytometer (BD Biosciences), with Annexin V-APC excited at 633 nm and PI at 488 nm. Data were acquired through CellQuest Pro software, recording at least 10,000 events per sample. FlowJo software was used to analyze the apoptotic rates, utilizing a gating strategy to exclude debris and doublets, ensuring accurate and reliable results.

MTT assay

786-O and A498 cells infected with lentivirus were plated in triplicate into five 96-well plates (2,000 cells/well). Each well was treated with 20 μL of 5 mg/mL MTT solution (GenView) for 4 h. 100 μL of DMSO was added to dissolve the resulting formazan

crystals. OD490 was measured using a Tecan microplate reader, and cell viability was determined based on the recorded absorbance values.

CCK8 assay

Logarithmic-growth-phase 786-O and A498 cells infected with lentivirus were detached by trypsin, then resuspended in their own media. These cells were seeded in triplicate into 96-well plates (2,000 cells/well). The next day, 10 μL of CCK-8 solution (Sigma) was added 2–4 h before the daily incubation finished. After a 4-h incubation, a Tecan microplate reader measured the OD450, and cell viability was calculated from the absorbance data.

Wound healing assay

Lentivirus-infected 786-O and A498 cells were plated in triplicate into 96-well plates (50,000 cells/well). After the cells formed a monolayer, a scratch was made across the surface. The cells were then incubated for 24 h, during which images were captured under a microscope after 8 or 24 h. The migration rate was determined according to the recorded images.

Colony formation assay

Lentivirus-infected 786-O and A498 cells were plated into 6-well plates (500 cells/well). 8 days later, following two PBS washes, the colonies were photographed with a camera. The colonies were then fixed using 4% paraformaldehyde and marked with Giemsa. Finally, distinct colonies were counted for evaluating colony formation ability of cells.

Transwell assay

Transwell chambers (Corning) were used to evaluate the migration capacity of lentivirus-infected cells. Exponentially growing 786-O and A498 cells were cultured in the upper chamber with serum-free medium for 24 h. The lower chamber was filled with medium supplemented with 30% FBS to serve as a chemoattractant. After non-migratory cells were removed, those that had migrated to the underside of the membrane were fixed with 4% formaldehyde and stained with 400 μL of Giemsa. The migratory capacity of the cells was then analyzed.

Human apoptosis antibody array

Protein samples extracted from 786-O cells in different groups were applied to Human Apoptosis Antibody Array (R&D Systems) for incubation at 4 °C following a blocking step. The membranes were then treated with HRP-conjugated Streptavidin for signal detection. Enhanced chemiluminescence (ECL) from Amersham was employed to visualize the signals, and their intensities were quantified using ImageJ.

Affymetrix human genechip primeview

Total RNA, qualified and integrated with Nanodrop 2000 spectrophotometer (Thermo Fisher Scientific) and 2100 Bioanalyzer (Agilent) were used for sequencing performed by Yibeirui (Shanghai, China) on the Affymetrix Human GeneChip PrimeView platform according to the manufacturer's instructions. Raw data were analyzed for statistical significance using the Welch t-test combined with Benjamini–Hochberg FDR correction, with $FDR < 0.05$ considered significant. Enrichment analysis was conducted through Ingenuity Pathway Analysis (Qiagen).

In vivoexperiments and fluorescence imaging

To establish a mouse xenograft model, 20 four-week-old female BALB/c nude mice (Lingchang, China) were randomly assigned to shCtrl and shMCM8 groups. Each mouse was subcutaneously injected with 4×10^6 shCtrl or shMCM8 ACHN cells. Tumor volume $= \pi/6 \times A \times B^2$, where A represents the longest diameter and B the perpendicular diameter. Tumor dimensions were recorded 2–3 times per week. Fluorescence imaging was conducted with IVIS Spectrum System (Perkin Elmer) after anesthetizing the mice with pentobarbital sodium (70 mg/kg). Finally, the mice were euthanized, tumors were collected, and paraffin-embedded sections were prepared for Ki-67 immunostaining. All procedures were conducted at the Animal Experiment Center of Nanjing Medical University.

Table 1 Expression patterns of MCM8 in renal carcinoma tissues and normal tissues revealed in immunohistochemistry analysis

MCM8 expression	Tumor tissue		Normal tissue	
	Cases	Percentage	Cases	Percentage
Low	34	50.7%	10	100%
High	33	49.3%	0	-

$P = 0.003$

Chromatin immunoprecipitation (ChIP)-qPCR

Chromatin extraction and ChIP assays were conducted using corresponding kits supplied by Abcam (Cambridge, MA, USA). The experiments were performed following the detailed instructions provided by the manufacturer. RT-PCR was carried out as previously described.

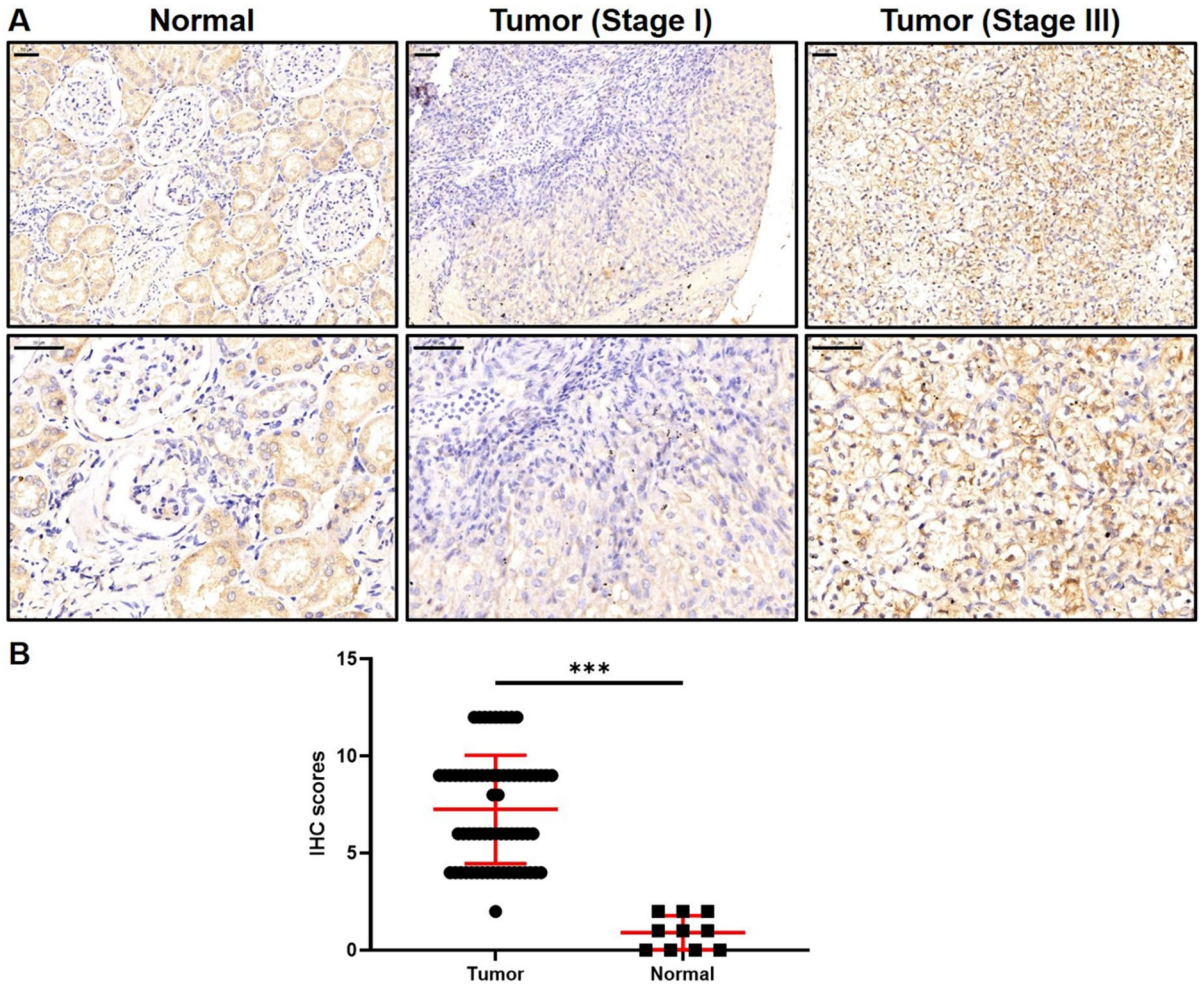

Fig. 1 MCM8 is upregulated in renal carcinoma tissues and associated with pathological stage. **A** IHC was performed to detect the expression of MCM8 in normal tissues and renal carcinoma tissues with different TNM stage (scale bar = 50 μm). **B** Based on IHC scores, the expression of MCM8 in renal carcinoma tissues and normal tissues were compared. *** $P < 0.001$

Table 2 Relationship between MCM8 expression and tumor characteristics in patients with renal carcinoma

Features	No. of patients	MCM8 expression		*P* value
		low	high	
All patients	67	34	33	
Age (years)				0.712
< 54	32	17	15	
≥ 54	35	17	18	
Gender				0.154
Male	43	19	24	
Female	24	15	9	
Grade				0.622
1	49	26	23	
2	14	7	7	
3	1	0	1	
Stage				< 0.001
I	14	11	3	
II	27	21	6	
III	24	2	22	
IV	2	0	2	

Dual-luciferase assay

The promoters of wild-type E2F1 (E2F1-WT) and its mutant variant (E2F1-Mut), where the sequence AGA AAGGTCAGT was altered to GAGGGAACAGAC , were inserted into the GL002 vector. These plasmids were transfected into 786-O cells, either with or without overexpression of MCM8 or NR4A1, under the help of Lipofectamine 3000. After 48 h, luciferase activity was assessed by following the protocol of the Promega Dual-Luciferase Reporter Assay Kit. Firefly luciferase activity was normalized to Renilla luciferase activity to calculate relative luciferase activity. To ensure reliability, all experiments were performed in triplicate.

ATP content, glucose content and lactate content detection assays

The ATP Content Testing Kit (product number #BC0300, Solarbio, China), Glucose Content Testing Kit (product number #BC2500, Solarbio, China), and Lactate Content Detection Kit (product number #BC2230, Solarbio, China) were employed to determine the levels of ATP, glucose, and lactate respectively. All operations were carried out in line with the instructions provided by the manufacturers.

Statistical analysis

Each experiment was repeated three times, and the outcomes are shown as the mean value plus or minus the standard deviation (SD). Different statistical methods were used for the evaluations, such as Student's t-test, Mann–Whitney U test, and Spearman Rank correlation analysis. These analyses were executed with SPSS 17.0 (IBM) and GraphPad Prism 9. If the P-value was less than 0.05, it was regarded as statistically significant.

Results

MCM8 is upregulated in renal carcinoma tissues and associated with pathological stage

MCM8 expression levels in renal carcinoma tissues were initially evaluated using immunohistochemistry (IHC) analysis. A tissue microarray (TMA) comprising 67 tumor samples from renal carcinoma patients and 10 normal tissue samples was constructed. Based on the median IHC scores, patients were divided into two groups: those with high MCM8 expression (33 out of 67 tumor tissues) and those with low MCM8 expression (34 tumor tissues and all normal samples). Normal tissues were exclusively classified as having low MCM8 expression (Table 1, $P < 0.001$). The findings revealed a significant increase in MCM8 expression in renal carcinoma tissues compared to normal counterparts (Fig. 1). Statistical analysis using Chi-square and Spearman rank correlation further indicated that elevated MCM8 levels were strongly associated with advanced pathological stages (Fig. 1A, Table 2, and Table S3, $P < 0.001$).

Knockdown of MCM8 inhibits cell growth, promotes cell apoptosis and suppresses cell migration

Next, lentivirus vectors tagged with GFP were used to transfect shMCM8 into 786-O and A498 renal carcinoma cells, establishing MCM8 knockdown models. Successful transfection was confirmed through fluorescence imaging (Figure S1). Furthermore, qPCR and western blot analyses revealed a significant MCM8

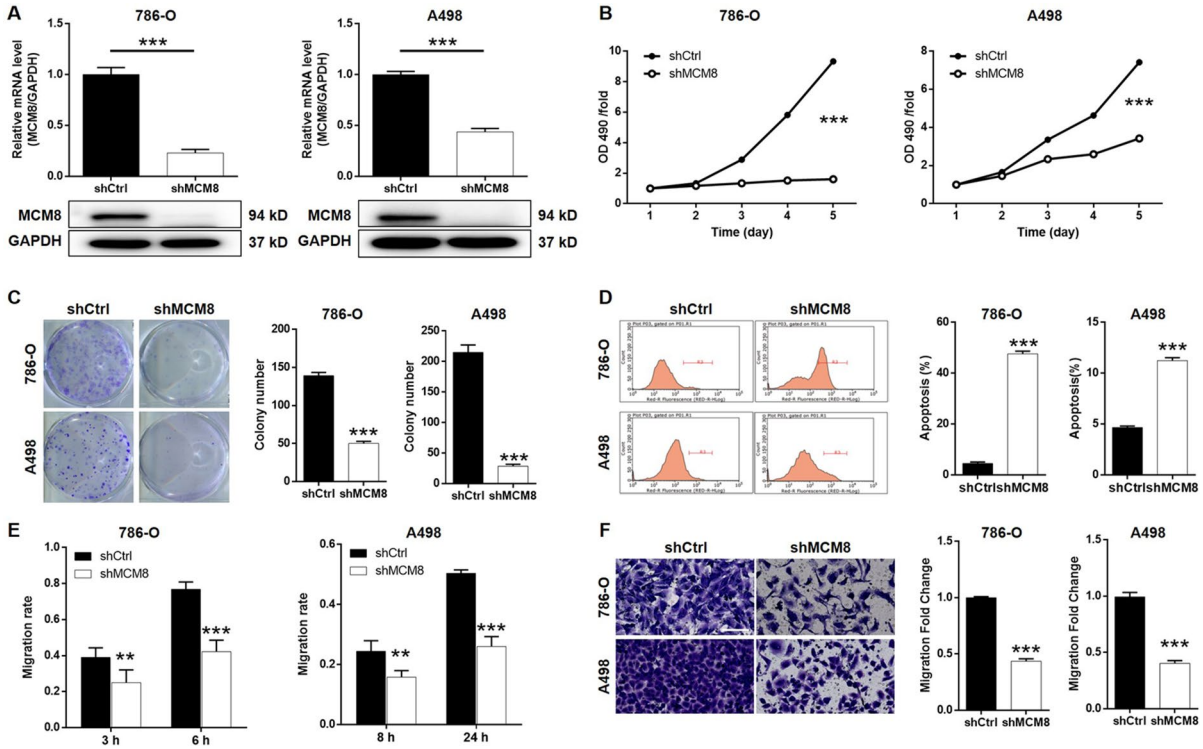

Fig. 2 Knockdown of MCM8 inhibits cell growth, promotes cell apoptosis and suppresses cell migration. **A** qPCR and western blotting were performed to confirm the knockdown of MCM8 by shMCM8 in 786-O and A498 cells. **B** Knockdown of MCM8 inhibited cell proliferation as detected by MTT assay. **C** Knockdown of MCM8 inhibited colony formation as detected by colony formation assay. **D** Knockdown of MCM8 promoted cell apoptosis as detected by flow cytometry. **E, F** Knockdown of MCM8 inhibited cell migration as detected by wound-healing (**E**) and Transwell assay (scale bar = 100 μm) (**F**). Data were presented as mean ± SD ($n \geq 3$). ** $P < 0.01$, *** $P < 0.001$

expression reduction in cells with shMCM8 transfection (Fig. 2A $P < 0.001$). Results from MTT assays indicated that MCM8 knockdown substantially suppressed cell proliferation (Fig. 2B $P < 0.001$), while colony formation was notably reduced (Fig. 2C $P < 0.001$). Flow cytometry analysis showed a marked increase in apoptosis in shMCM8-treated cells (Fig. 2D $P < 0.001$). Moreover, elevated levels of apoptosis-related proteins, including CD40, CD40L, cytoC, DR6, Fas, FasL, HTRA, p21, p27, p53, and SMAC, were detected after MCM8 silencing (Figure S2A-S2C, $P < 0.05$). The impact of MCM8 on cell motility was assessed, both wound-healing and Transwell assays demonstrated reduced migratory ability in MCM8-deficient cells (Fig. 2E-F $P < 0.001$). Together, these findings highlight the critical involvement of MCM8 in promoting renal carcinoma progression.

Knockdown of MCM8 suppresses tumor growth in vivo

Next, 786-O cells with or without MCM8 silencing were used for constructing subcutaneous xenograft models. Tumor growth was evaluated through analyses of growth curves, measurements of tumor volume and weight, in vivo imaging, and photographic documentation of dissected tumors. The results consistently showed that MCM8 knockdown slowed down tumor growth (Fig. 3A-E $P < 0.001$). Furthermore, immunohistochemical analysis revealed reduced Ki-67 expression in the shMCM8 group, indicating diminished cell proliferation (Fig. 3F). These findings underscore the significant role of MCM8 knockdown in inhibiting renal carcinoma progression in vivo.

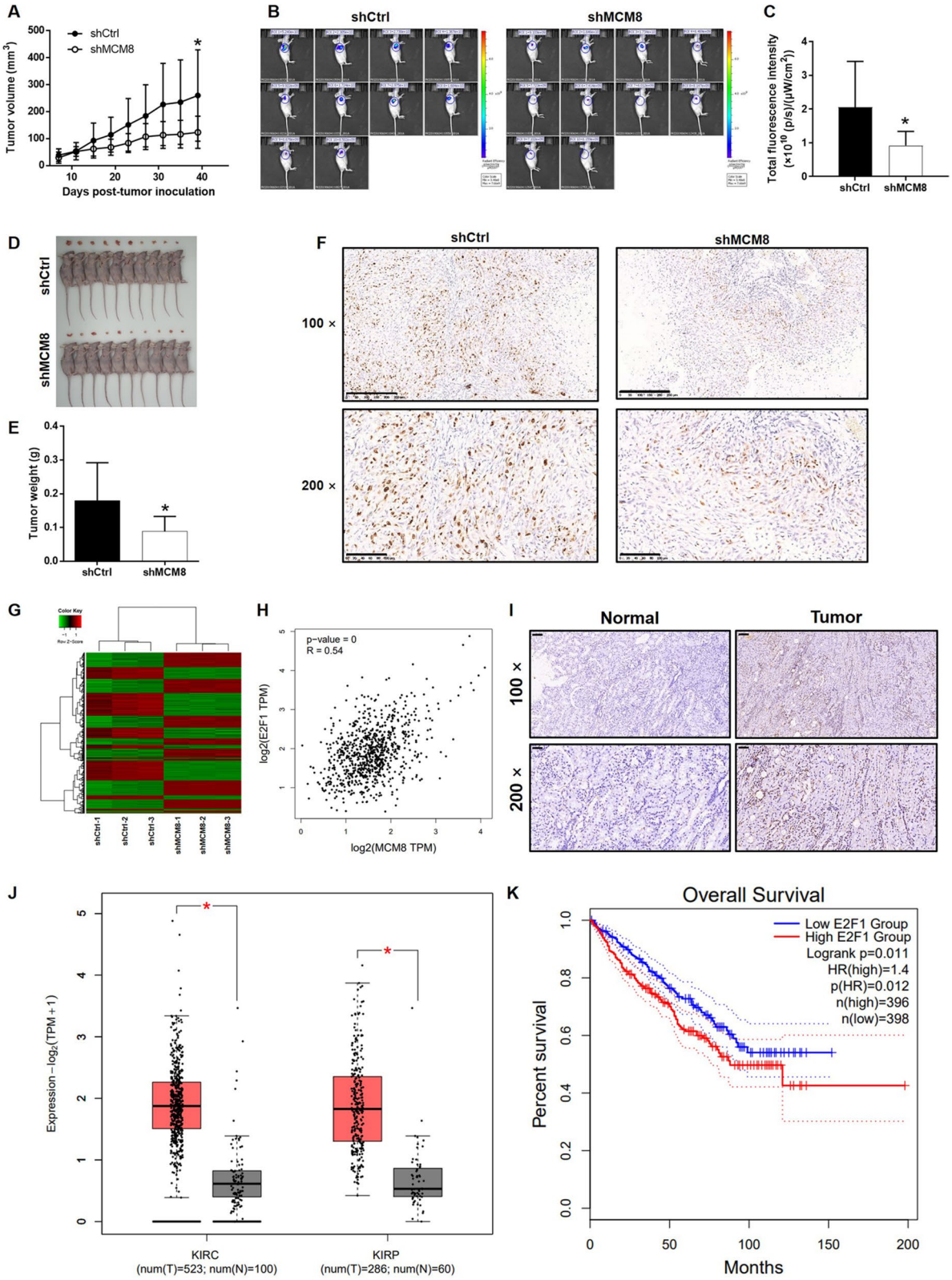
A
shCtrl
shMCM8
Tumor volume (mm3)
Days post-tumor inoculation
B
shCtrl
shMCM8
C
Total fluorescence intensity (×10^10 (p/s)/(μW/cm2))
shCtrl
shMCM8
D
shCtrl
shMCM8
E
Tumor weight (g)
shCtrl
shMCM8
F
shCtrl
shMCM8
100 ×
200 ×
G
Color Key
shCtrl-1
shCtrl-2
shCtrl-3
shMCM8-1
shMCM8-2
shMCM8-3
H
p−value = 0
R = 0.54
log2(E2F1 TPM)
log2(MCM8 TPM)
I
Normal
Tumor
100 ×
200 ×
J
Expression – log2(TPM + 1)
KIRC
(num(T)=523; num(N)=100)
KIRP
(num(T)=286; num(N)=60)
K
Overall Survival
Low E2F1 Group
High E2F1 Group
Logrank p=0.011
HR(high)=1.4
p(HR)=0.012
n(high)=396
n(low)=398
Percent survival
Months

◂**Fig. 3** Knockdown of MCM8 suppresses tumor growth in vivo. **A** Xenografts formed by shMCM8 cells grew slower than that formed by shCtrl cells. **B** In vivo imaging was performed to estimate the tumor burden of mice. **C** The bioluminescence intensity was scanned as a representation of tumor burden. **D** Photos of mice and tumors were taken after sacrificing the mice and collecting the tumors. **E** The removed xenografts were collected and weighted. **F** IHC was performed to detect the expression of Ki-67 in sections of xenografts (scale bar = 250 μm for 100× images and 100 μm for 200× images). **G** Gene expression profiling analysis was performed to identify differentially expressed genes between shCtrl and shMCM8 cells. **H** The correlation between MCM8 and E2F1 expression was analyzed based on TCGA database (KIRC + KIRP datasets). **I** IHC was performed to detect the expression of E2F1 in normal and renal carcinoma tissues (scale bar = 100 μm for 100× images and 50 μm for 200× images). Data were presented as mean ± SD ($n \geq 3$). **J** The differential expression of E2F1 in renal carcinoma tissues and normal tissues was analyzed based on TCGA database (KIRC + KIRP datasets). **K** The survival analysis was performed based on TCGA database (KIRC + KIRP datasets) to reveal the association between E2F1 expression and renal carcinoma patients. Data were presented as mean ± SD ($n \geq 3$). * $P < 0.05$

Knockdown of MCM8 inhibits renal carcinoma through downregulating E2F1

To investigate how MCM8 regulates renal carcinoma, gene expression profiles in 786-O cells with and without MCM8 knockdown were detected and compared. 3415 differentially expressed genes (DEGs, |Fold Change| ≥ 1.3) were recognized, comprising 1263 upregulated and 1152 downregulated genes in shMCM8 cells (Fig. 3G, S3A, and S3B). Subsequent IPA database enrichment analysis (Figure S3C and S3D) highlighted several significantly impacted DEGs, which were further validated by qPCR and western blot assays. As shown in Figure S4A-S4B, both mRNA and protein levels of E2F1, categorized under "Cancer" in IPA analysis (Figure S3D), were significantly reduced in shMCM8 cells. IPA analysis also suggested a regulatory link between MCM8 and E2F1, identifying E2F1 as a likely downstream target

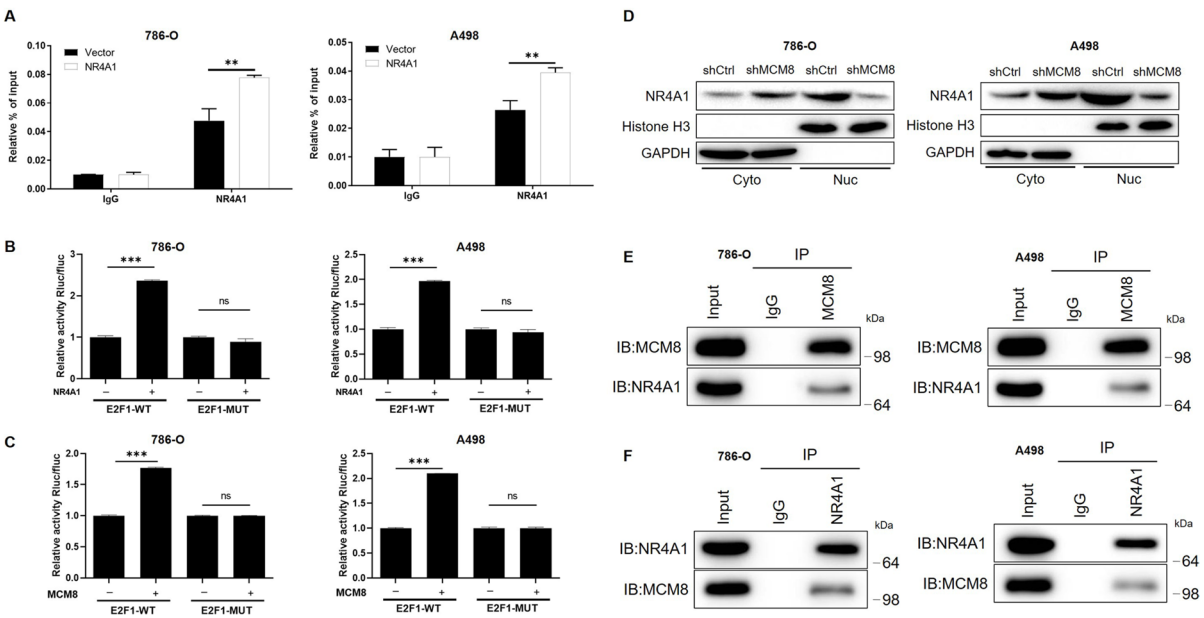

Fig. 4 MCM8 regulates renal carcinoma through affecting NR4A1-mediated E2F1 transcription. **A** ChIP-qPCR was used to confirm the interaction between NR4A1 and E2F1 promotor in 786-O and A498 cells with or without MCM8 knockdown. **B-C** 786-O and A498 cells were co-transfected with E2F1-WT promotor or E2F1-MUT promotor luciferase reporter and NR4A1 (**B**) or MCM8 (**C**) overexpression plasmids followed by analysis of luciferase activity. **D** Western blot analysis of NR4A1 in cytoplasmic and nucleus fractions of 786-O and A498 cells with or without MCM8 knockdown. Histone H3 and GAPDH were used as nucleus and cytoplasmic markers, respectively. **E** Cell lysates of 786-O and A498 cells were immunoprecipitated with IgG or MCM8 antibodies, and immunoblot assays were performed using MCM8 or NR4A1 antibodies. **F** Cell lysates of 786-O and A498 cells were immunoprecipitated with IgG or NR4A1 antibodies, and immunoblot assays were performed using MCM8 or NR4A1 antibodies. Data were presented as mean ± SD ($n \geq 3$). ** $P < 0.01$, *** $P < 0.001$

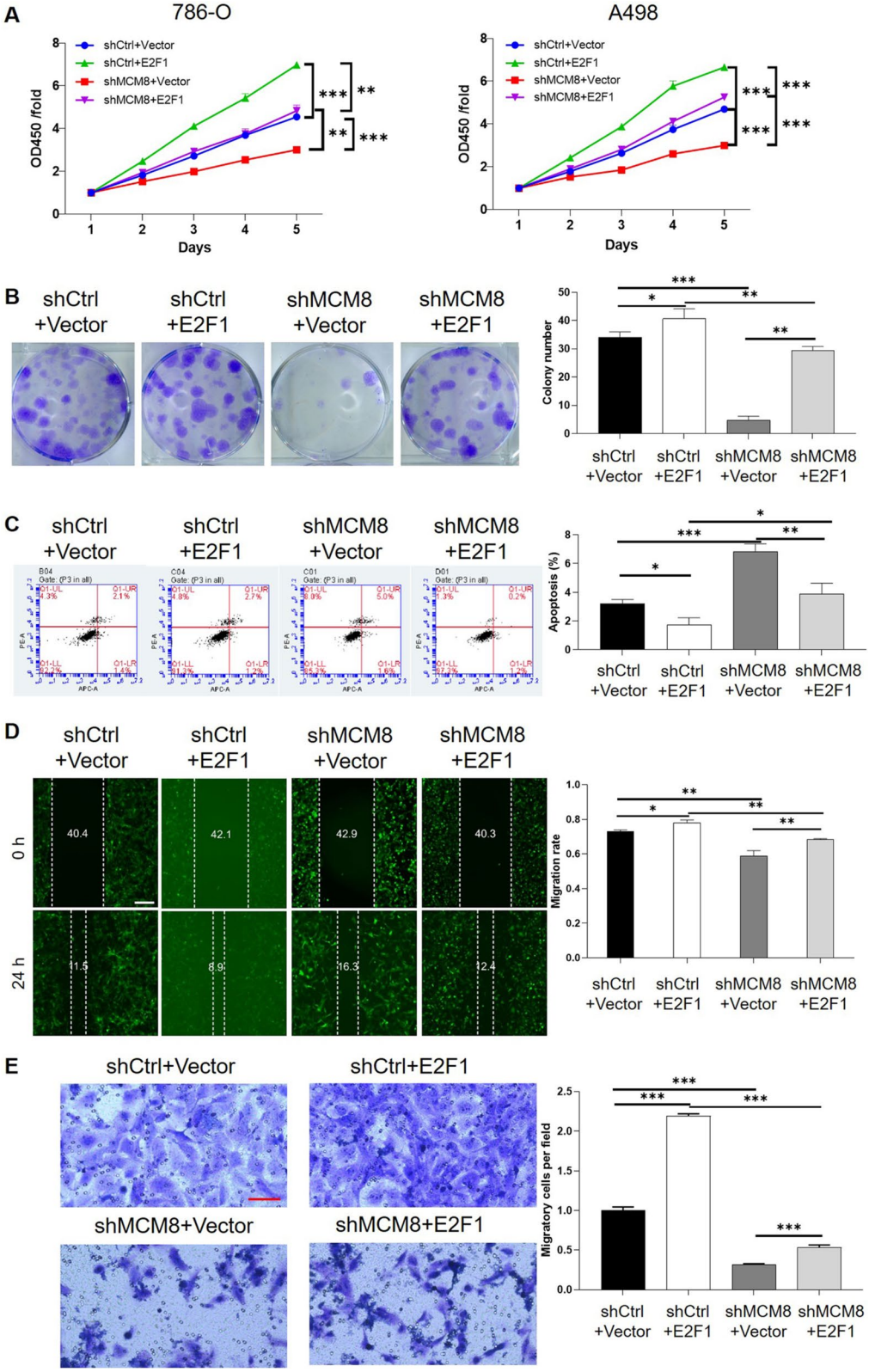
A
786-O
A498
shCtrl+Vector
shCtrl+E2F1
shMCM8+Vector
shMCM8+E2F1
OD450 /fold
Days
B
shCtrl +Vector
shCtrl +E2F1
shMCM8 +Vector
shMCM8 +E2F1
Colony number
C
Apoptosis (%)
D
0 h
24 h
40.4
42.1
42.9
40.3
11.5
8.9
16.3
12.4
Migration rate
E
Migratory cells per field

◂**Fig. 5** Overexpression of E2F1 alleviates the inhibition of renal carcinoma development induced by MCM8 knockdown. **A** CCK8 assay was utilized to detect the effects of mere E2F1 overexpression or mere MCM8 knockdown or simultaneous E2F1 overexpression and MCM8 knockdown on cell proliferation of 786-O and A498 cells. **B** Colony formation assay was utilized to detect the effects of mere E2F1 overexpression or mere MCM8 knockdown or simultaneous E2F1 overexpression and MCM8 knockdown on colony formation of 786-O cells. **C** Flow cytometry was utilized to detect the effects of mere E2F1 overexpression or mere MCM8 knockdown or simultaneous E2F1 overexpression and MCM8 knockdown on cell apoptosis of 786-O cells. **D, E** Wound-healing (scale bar = 200 μm) (**D**) and Transwell (scale bar = 100 μm) (**E**) assays were used to detect the effects of mere E2F1 overexpression or mere MCM8 knockdown or simultaneous E2F1 overexpression and MCM8 knockdown on cell migration of 786-O cells. Data were presented as mean ± SD ($n \geq 3$). * $P < 0.05$, ** $P < 0.01$, *** $P < 0.001$

of MCM8 in renal carcinoma (Figure S4C). Correlation analysis using TCGA datasets (KIRC + KIRP) revealed the positive correlation between MCM8 and E2F1 in renal carcinoma (Fig. 3H). Furthermore, IHC analysis confirmed that E2F1 levels were elevated in renal carcinoma tissues, resembling the MCM8 expression trend (Fig. 3I). In the KIRC and KIRP datasets, similar trend was also found for E2F1 expression (Fig. 3J), and its upregulation was associated with poor patient prognosis (Fig. 3K). These findings suggest that E2F1 acts as a key cofactor in the regulatory effects of MCM8 on renal carcinoma.

MCM8 interacts with NR4A1 and affects NR4A1-mediated transcription of E2F1

Considering the regulatory influence of MCM8 on the levels of E2F1 mRNA and protein, we postulated that MCM8 might regulate E2F1 expression through modulating its transcription. For this purpose, the TRRUST database was employed, and NR4A1 was identified as a potential transcription factor for E2F1. This prediction was verified by chromatin immunoprecipitation (ChIP) assays, which demonstrated the binding of NR4A1 to the E2F1 promoter region (Fig. 4A), thus confirming its role in transcriptional regulation. The predicted binding sites on the E2F1 promoter (Figure S5) directed dual-luciferase assays. In these assays, the overexpression of either MCM8 or NR4A1 remarkably enhanced the activity of the E2F1 promoter (Fig. 4B-C). However, this effect was mostly eliminated when the binding site was mutated. Further experiments indicated that the knockdown of MCM8 decreased the nuclear levels of NR4A1 (Fig. 4D), suggesting an association between MCM8 and the nuclear localization of NR4A1. Co-immunoprecipitation assays validated a physical interaction between MCM8 and NR4A1, as shown by the distinct bands (Fig. 4E-F). Collectively, these results suggest a mechanism in which MCM8 modulates the nuclear localization of NR4A1, consequently influencing E2F1 transcription.

MCM8 and E2F1 synergistically regulates renal carcinoma development

To investigate the effects of MCM8/E2F1 axis on renal carcinoma progression, 786-O cell models were created by combining MCM8 knockdown with either E2F1 knockdown (shE2F1-2, Figure S6) or E2F1 overexpression. The effectiveness of MCM8 and E2F1 knockdown was evaluated through qPCR (Figure S7). As demonstrated by cell phenotype assays (Figure S8A-S8E), E2F1 knockdown inhibited the progression of renal carcinoma and strengthened the inhibitory impacts of MCM8 knockdown. Significantly, E2F1 overexpression promoted cell growth, motility, and decreased apoptosis. It also partially alleviated the suppression of malignant phenotypes caused by MCM8 knockdown (Fig. 5 and S9).

MCM8/E2F1 axis may promote renal carcinoma development through facilitating aerobic glycolysis

This study also examined how MCM8 knockdown impacts the Akt signaling pathway. The results revealed that silencing MCM8 inhibited Akt phosphorylation and downregulated downstream effectors (Figure S10). Since both E2F1 and the Akt pathway are involved in regulating aerobic glycolysis in tumors, the connection between the MCM8/E2F1 axis and glycolysis was further investigated. As shown in Fig. 6A-B, MCM8 knockdown significantly lowered ATP, glucose, and lactate levels in renal carcinoma cells, indicating diminished glycolytic activity. Rescue experiments demonstrated that overexpressing E2F1 counteracted the reductions in ATP, glucose, and lactate induced by MCM8 knockdown (Fig. 6C-D). Conversely, overexpression of MCM8 elevated ATP, glucose, and lactate levels, an effect that was mitigated by E2F1 knockdown

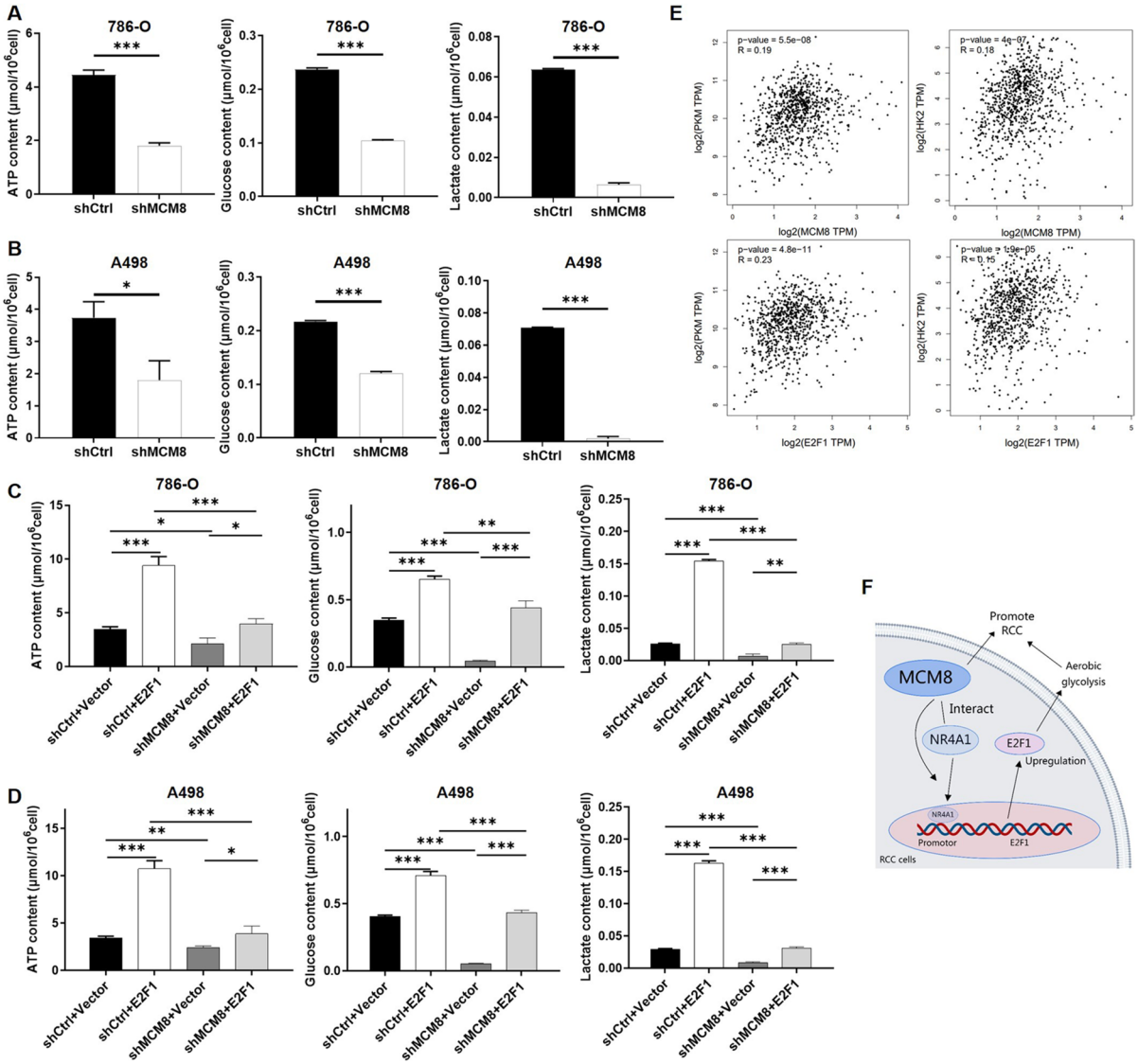

Fig. 6 MCM8/E2F1 axis may promote renal carcinoma development through facilitating aerobic glycolysis. **A-B** The ATP content, glucose content and lactate content in 786-O cells (**A**) and A498 cells (**B**) with or without MCM8 knockdown were detected by corresponding kits. **C-D** The ATP content, glucose content and lactate content in 786-O cells (**C**) and A498 cells (**D**) with mere E2F1 overexpression or mere MCM8 knockdown or simultaneous E2F1 overexpression and MCM8 knockdown. **E** The correlation between MCM8/E2F1 expression and PKM2/HK2 expression was analyzed based on TCGA database (KIRC + KIRP datasets). (F) Diagram of the proposed mechanism. Data were presented as mean ± SD ($n \geq 3$). * $P < 0.05$, ** $P < 0.01$, *** $P < 0.001$

(Figure S11). Additionally, correlation analysis using TCGA datasets (KIRC + KIRP) revealed strong positive relationships between MCM8/E2F1 and glycolysis-related enzymes such as PKM2 (PKM) and HK2 (Fig. 6E). Together, these findings suggest that the MCM8/E2F1 axis facilitates renal carcinoma progression by enhancing aerobic glycolysis.

Discussion

The minichromosome maintenance (MCM) complex family encompasses proteins that are essential for physiological activities. Nevertheless, its function in cancer development has not been fully elucidated. Li et al. (Li et al. 2019b) conducted a comprehensive examination of the prognostic significance of MCM proteins in lung adenocarcinoma (LUAD). The study revealed elevated mRNA expression of MCM2, MCM4, and MCM10 in LUAD, which was associated with poorer patient outcomes in LUAD. Regarding the biological functions of MCM8, most research has primarily focused on its role in DNA repair (Lee et al. 2015). For example, Lutzmann et al. (Lutzmann et al. 2019) demonstrated that deficiencies in MCM8 or MCM9 could result in p53-dependent myeloid tumorigenesis due to persistent hematopoietic DNA damage. Morii et al. (Morii et al. 2019) reported that disrupting the MCM8-MCM9 complex by knocking out MCM9 or silencing MCM8 enhanced efficiencies of cisplatin and the DNA repair inhibitor olaparib. Besides its involvement in DNA damage repair and drug resistance, recent studies have explored the regulatory influence of MCM8 on cancer cell malignancy. Duan et al. (Hao et al. 2021) determined that high MCM8 expression in cholangiocarcinoma (CCA) was a predictor of disease progression, and silencing MCM8 remarkably inhibited CCA cell malignancy and tumor development. In a similar vein, Zhu et al. (Zhu et al. 2021) showed that knockdown of MCM8 suppressed bladder cancer cell malignancy. In the present study, MCM8 was found to be a crucial regulator in renal carcinoma progression. It exhibited elevated expression in tumor tissues and was related to malignancy. Silencing MCM8 efficiently decreased cell proliferation and tumor growth in renal carcinoma.

Previous studies have explored some of the downstream mechanisms of MCM8 in malignant tumor regulation. For example, Ren et al. (Ren et al. 2021) found that MCM8 served as a key tumor-promoting factor in osteosarcoma and proposed CTGF as a potential co-factor in osteosarcoma progression, although the underlying molecular mechanism was not clear. In this research, E2F1 was identified as a downstream target of MCM8. Functionally, depleting E2F1 had similar inhibitory effects on renal carcinoma progression as MCM8 knockdown, and it further strengthened the regulatory influence on cell phenotypes. Conversely, overexpressing E2F1 alleviated the suppression of renal carcinoma development induced by MCM8 knockdown. Mechanistically, MCM8 seems to boost NR4A1-mediated E2F1 transcription by interacting with NR4A1 and facilitating its nuclear expression.

E2F1, a vital member of the E2F transcription factor family, controls processes like cell cycle progression, DNA replication and repair, differentiation, proliferation, and apoptosis. Many studies have indicated that E2F1 is highly expressed and promotes tumor development in various cancers (Gu et al. 2018; Wang et al. 2017; Liu et al. 2018; Wu and Yu 2009; Ertosun et al. 2016). For instance, Zheng et al. (Zheng et al. 2020) showed that silencing E2F1 upregulated miR-34c, making gastric cancer cells more sensitive to paclitaxel and cisplatin treatment. Similarly, Li et al. (Li et al. 2019a) reported the key role of E2F1 in laryngeal squamous cell carcinoma (LSCC), which has a significant impact on tumor progression. E2F1 regulates apoptosis through both p53-dependent and p53-independent pathways (Bell and Ryan 2004). In the p53-dependent pathway, E2F1 activates p14/p19, preventing p53 degradation and resulting in high p53 expression. This high p53 expression inhibits cyclin-dependent kinases (CDKs), disrupts the cell cycle, and induces apoptosis. Correspondingly, in MCM8-knockdown renal carcinoma cells, we observed elevated p53 levels and reduced CDK1 expression.

Moreover, the Akt signaling pathway, which is crucial for tumor progression, was inactivated in cells with MCM8 knockdown. This was accompanied by a decline in the expression of downstream effectors CCNB1 and CCND1 (Nitulescu et al. 2018; Song et al. 2019; Zhang et al. 2018; Zhen et al. 2017; Zhu et al. 2018). These results imply that E2F1, as a downstream target of MCM8, modulates renal carcinoma cell proliferation and apoptosis through the p53-dependent pathway and affects tumor progression via the Akt signaling.

The partial restoration of tumor growth when E2F1 is overexpressed after MCM8 knockdown indicates the participation of other MCM8 co-factors in regulating renal carcinoma cell functions. Besides E2F1, we noticed a decrease in Akt pathway activity following MCM8 knockdown. The Akt pathway, which has been extensively investigated as a characteristic of malignant tumors, is known to regulate aerobic

glycolysis (Paul et al. 2022; Yuan et al. 2022). Also, E2F1 is regarded as an upstream regulator of glycolysis, contributing to its role in promoting tumors. For instance, Ma et al. showed that E2F1 transcriptionally regulates SEC61G expression, influencing glycolysis in breast cancer and underlining its significance in tumorigenesis and as a potential therapeutic target (Ma et al. 2021). Likewise, Zhao et al. reported that E2F1 enhances glycolysis in LSCC, suggesting a possible approach for LSCC treatment (Zhao et al. 2022). Correspondingly, the MCM8/E2F1 axis exhibited clear regulatory effects on the levels of ATP, glucose, and lactate in renal carcinoma cells, stressing the importance of aerobic glycolysis as a downstream mechanism mediating the influence of MCM8/E2F1 on renal carcinoma progression.

In conclusion, this research emphasizes the vital role of MCM8 in renal cell carcinoma (RCC) progression (Fig. 6F). By clarifying the interaction between MCM8 and E2F1, we disclose a new mechanism underlying RCC development, which entails abnormal aerobic glycolysis. These findings not only deepen our comprehension of RCC pathogenesis but also offer valuable perspectives for devising targeted therapies against this malignancy.

Acknowledgements None.

Authors' contributions P.S. designed this program. All authors except P.S. operated the cell and animal experiments. X.W. and C.L. conducted the data collection and analysis. S.Z. produced the manuscript which was checked by P.S. All the authors have confirmed the submission of this manuscript.

Funding This work was financially supported by Key Research and Development Project of Jiangsu Province (BE2018749).

Data Availability No datasets were generated or analysed during the current study.

Declarations

Ethics approval and consent to participate This research was performed abiding by Ethics committee of the First Affiliated Hospital of Nanjing Medical University.

Consent for publication Not applicable.

Competing interests The authors declare no competing interests.

Clinical trial number Not applicable.

References

Bell LA, Ryan KM. Life and death decisions by E2F–1. Cell Death Differ. 2004;11:137–42.

Deegan TD, Diffley JF. MCM: one ring to rule them all. Curr Opin Struct Biol. 2016;37:145–51.

Ertosun MG, Hapil FZ, Osman Nidai O. E2F1 transcription factor and its impact on growth factor and cytokine signaling. Cytokine Growth Factor Rev. 2016;31:17–25.

Golijanin B, Malshy K, Khaleel S, Lagos G, Amin A, Cheng L, Golijanin D, Mega A. Evolution of the HIF targeted therapy in clear cell renal cell carcinoma. Cancer Treat Rev. 2023;121:102645.

Gu Y, Wang X, Liu H, Li G, Yu W, Ma Q. SET7/9 promotes hepatocellular carcinoma progression through regulation of E2F1. Oncol Rep. 2018;40:1863–74.

Hao J, Deng H, Yang Y, Chen L, Wu Q, Yao P, Li J, Li B, Jin X, Wang H, Duan H. Downregulation of MCM8 expression restrains the malignant progression of cholangiocarcinoma. Oncol Rep. 2021;46:1–11.

Lee KY, Im JS, Shibata E, Park J, Handa N, Kowalczykowski SC, Dutta A. MCM8-9 complex promotes resection of double-strand break ends by MRE11-RAD50-NBS1 complex. Nat Commun. 2015;6:7744.

Li P, Lin XJ, Yang Y, Yang AK, Di JM, Jiang QW, Huang JR, Yuan ML, Xing ZH, Wei MN, Li Y, Yuan XH, Shi Z, Liu H, Ye J. Reciprocal regulation of miR-1205 and E2F1 modulates progression of laryngeal squamous cell carcinoma. Cell Death Dis. 2019a;10:916.

Li S, Jiang Z, Li Y, Xu Y. Prognostic significance of minichromosome maintenance mRNA expression in human lung adenocarcinoma. Oncol Rep. 2019b;42:2279–92.

Liu ZL, Bi XW, Liu PP, Lei DX, Wang Y, Li ZM, Jiang WQ, Xia Y. Expressions and prognostic values of the E2F

transcription factors in human breast carcinoma. Cancer Manag Res. 2018;10:3521–32.
Lutzmann M, Bernex F, da Costa C, de Jesus D, Hodroj C, Marty I, Plo W, Vainchenker M, Tosolini L, Forichon C, Bret S, Queille C, Marchive JSH, Méchali M. MCM8- and MCM9 Deficiencies Cause Lifelong Increased Hematopoietic DNA Damage Driving p53-Dependent Myeloid Tumors. Cell Rep. 2019;28:2851-2865.e2854.
Ma J, He Z, Zhang H, Zhang W, Gao S, Ni X. SEC61G promotes breast cancer development and metastasis via modulating glycolysis and is transcriptionally regulated by E2F1. Cell Death Dis. 2021;12:550.
Meng L, Collier KA, Wang P, Li Z, Monk P, Mortazavi A, Hu Z, Spakowicz D, Zheng L, Yang Y. Emerging Immunotherapy Approaches for Advanced Clear Cell Renal Cell Carcinoma. Cells. 2023;13:34.
Miller KD, Nogueira L, Devasia T, Mariotto AB, Yabroff KR, Jemal A, Kramer J, Siegel RL. Cancer treatment and survivorship statistics, 2022. CA Cancer J Clin. 2022;72:409–36.
Morii I, Iwabuchi Y, Mori S, Suekuni M, Natsume T, Yoshida K, Sugimoto N, Kanemaki MT, Fujita M. Inhibiting the MCM8-9 complex selectively sensitizes cancer cells to cisplatin and olaparib. Cancer Sci. 2019;110:1044–53.
Nishimura K, Ishiai M, Horikawa K, Fukagawa T, Takata M, Takisawa H, Kanemaki MT. Mcm8 and Mcm9 form a complex that functions in homologous recombination repair induced by DNA interstrand crosslinks. Mol Cell. 2012;47:511–22.
Nitulescu GM, Van De Venter M, Nitulescu G, Ungurianu A, Juzenas P, Peng Q, Olaru OT, Grădinaru D, Tsatsakis A, Tsoukalas D, Spandidos DA, Margina D. The Akt pathway in oncology therapy and beyond (Review). Int J Oncol. 2018;53:2319–31.
Park J, Long DT, Lee KY, Abbas T, Shibata E, Negishi M, Luo Y, Schimenti JC, Gambus A, Walter JC, Dutta A. The MCM8-MCM9 complex promotes RAD51 recruitment at DNA damage sites to facilitate homologous recombination. Mol Cell Biol. 2013;33:1632–44.
Paul S, Ghosh S, Kumar S. Tumor glycolysis, an essential sweet tooth of tumor cells. Semin Cancer Biol. 2022;86:1216–30.
Posadas EM, Limvorasak S, Figlin RA. Targeted therapies for renal cell carcinoma. Nat Rev Nephrol. 2017;13:496–511.
Ren Z, Li J, Zhao S, Qiao Q, Li R. Knockdown of MCM8 functions as a strategy to inhibit the development and progression of osteosarcoma through regulating CTGF. Cell Death Dis. 2021;12:376.
Rizzo M, Caliò A, Brunelli M, Pezzicoli G, Ganini C, Martignoni G, Camillo P. Clinico-pathological implications of the 2022 WHO Renal Cell Carcinoma classification. Cancer Treat Rev. 2023;116: 102558.
Siegel RL, Giaquinto AN, Jemal A. Cancer statistics, 2024. CA Cancer J Clin. 2024;74:12–49.
Singh D. Current updates and future perspectives on the management of renal cell carcinoma. Life Sci. 2021;264: 118632.
Song M, Bode AM, Dong Z, Lee MH. AKT as a Therapeutic Target for Cancer. Cancer Res. 2019;79:1019–31.
Sung H, Ferlay J, Siegel RL, Laversanne M, Soerjomataram I, Jemal A, Bray F. Global Cancer Statistics 2020: GLOBOCAN Estimates of Incidence and Mortality Worldwide for 36 Cancers in 185 Countries. CA Cancer J Clin. 2021;71:209–49.
Wang T, Chen X, Qiao W, Kong L, Sun D, Li Z. Transcription factor E2F1 promotes EMT by regulating ZEB2 in small cell lung cancer. BMC Cancer. 2017;17:719.
Wolf MM, KimrynRathmell W, Beckermann KE. Modeling clear cell renal cell carcinoma and therapeutic implications. Oncogene. 2020;39:3413–26.
Wu Z, Yu Q. E2F1-mediated apoptosis as a target of cancer therapy. Curr Mol Pharmacol. 2009;2:149–60.
Yuan Y, Li H, Pu W, Chen L, Guo D, Jiang H, He B, Qin S, Wang K, Li N, Feng J, Wen J, Cheng S, Zhang Y, Yang W, Ye D, Lu Z, Huang C, Mei J, Zhang HF, Gao P, Jiang P, Su S, Sun B, Zhao SM. Cancer metabolism and tumor microenvironment: fostering each other? Sci China Life Sci. 2022;65:236–79.
Zhang Y, Xia F, Liu X, Yu Z, Xie L, Liu L, Chen C, Jiang H, Hao X, He X, Zhang F, Gu H, Zhu J, Bai H, Zhang CC, Chen GQ, Zheng J. JAM3 maintains leukemia-initiating cell self-renewal through LRP5/AKT/β-catenin/CCND1 signaling. J Clin Invest. 2018;128:1737–51.
Zhao L, Zheng Y, Zhang L, Su L. E2F1-Induced FTH1P3 Promoted Cell Viability and Glycolysis Through miR-377-3p/LDHA Axis in Laryngeal Squamous Cell Carcinoma. Cancer Biother Radiopharm. 2022;37:276–86.
Zhen Y, Fang W, Zhao M, Luo R, Liu Y, Fu Q, Chen Y, Cheng C, Zhang Y, Liu Z. miR-374a-CCND1-pPI3K/AKT-c-JUN feedback loop modulated by PDCD4 suppresses cell growth, metastasis, and sensitizes nasopharyngeal carcinoma to cisplatin. Oncogene. 2017;36:275–85.
Zheng H, Wang JJ, Yang XR, Yu YL. Upregulation of miR-34c after silencing E2F transcription factor 1 inhibits paclitaxel combined with cisplatin resistance in gastric cancer cells. World J Gastroenterol. 2020;26:499–513.
Zhu X, Li Z, Li T, Long F, Lv Y, Liu L, Liu X, Zhan Q. Osthole inhibits the PI3K/AKT signaling pathway via activation of PTEN and induces cell cycle arrest and apoptosis in esophageal squamous cell carcinoma. Biomed Pharmacother. 2018;102:502–9.
Zhu W, Gao F, Zhou H, Jin K, Shao J, Xu Z. Knockdown of MCM8 inhibits development and progression of bladder cancer in vitro and in vivo. Cancer Cell Int. 2021;21:242.